Influence of Variable Leg Elasticity on the Stability of Quadrupedal Gaits

Federico Del Fatti[1], Anna Sesselmann[2] and Máximo A. Roa[2]

***Abstract*— Several template models have been developed to facilitate the analysis of limit-cycles for quadrupedal locomotion. The parameters in the model are usually fixed; however, biology shows that animals change their leg stiffness according to the locomotion velocity, and this adaptability invariably affects the stability of the gait. This paper provides an analysis of the influence of this variable leg stiffness on the stability of different quadrupedal gaits. The analysis exploits a simplified quadrupedal model with compliant legs and shoulder joints represented as torsional springs. This model can reproduce the most common quadrupedal gaits observed in nature. The stability of such emerging gaits is then checked. Afterward, an optimization process is used to search for the system parameters that guarantee maximum gait stability. Our study shows that using the highest feasible leg swing frequency and adopting a leg stiffness that increases with the speed of locomotion noticeably improves the gait stability over a wide range of horizontal velocities while reducing the oscillations of the trunk. This insight can be applied in the design of novel elastic quadrupedal robots, where variable stiffness actuators could be employed to improve the overall locomotion behavior.**

I. Introduction

The interest in legged robots has rapidly increased in the past decades. They are an interesting solution for executing dull, dirty or dangerous tasks while operating in rough terrains. The development of such robots is very demanding in terms of structural design and control complexity, so natural solutions are often used as a source of inspiration. Animals display different walking or running behaviors depending on the velocity of locomotion [1]. The analysis of such gait selection process according to the natural morphological configurations is still an ongoing research area [2], [3]. Animals use compliant elements, such as tendons and muscles, to store and release energy during the stride, thus increasing locomotion efficiency [4]. This finding inspired a new generation of robots implementing compliant elements acting in parallel to the leg actuators, including for instance the DLR quadrupedal robot Bert (Fig. 1), ANYmal, developed by ANYbotics [5] and StarlETH, developed by ETH [6].

Different template models implementing compliant legs have been developed, attempting to explain and reproduce the gaits observed in nature. The SLIP (Spring Linear Inverted Pendulum) model, characterized by a point mass attached to a single massless compliant leg, reproduces running and hopping gaits [7]. Introducing a second massless leg allows to characterize also the walking gaits [8]. However, the described models do not include the influence of the leg swing, but instead, consider an instantaneous return of the leg to a predefined angle of attack. To characterize the passive swing of the legs in bipedal gait, a torsional hip stiffness and a foot mass for each leg were introduced [9]. This model was extended to the quadrupedal case by introducing another pair of legs and a rigid trunk [10]. All of the above models can reproduce the most common bipedal and quadrupedal gaits observed in nature, without needing an active control mechanism. Following these ideas, the implementation of robots with inherent passive locomotion gaits increases energy efficiency and reduces the effort required for the gait control [2], [11]. Adopting gaits with higher stability further simplifies the control problem.

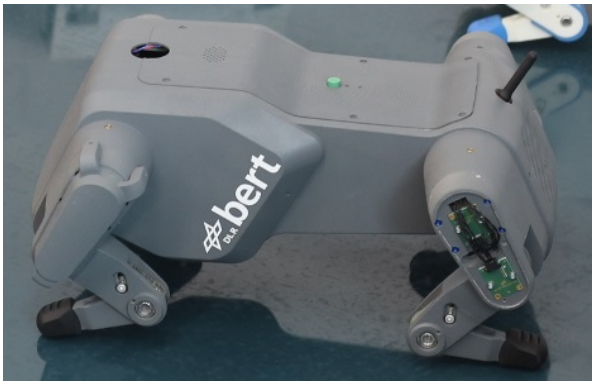

Fig. 1: Quadrupedal robot Bert, developed at DLR.

All of the above models utilize a fixed set of parameters for analyzing the locomotion behaviors. However, empirical studies in animals have shown that leg stiffness is not fixed, but it changes with the horizontal velocity, suggesting that the introduction of variable stiffness could be fundamental to improve the stability in a wide range of velocities [12]. Furthermore, technology nowadays allows manufacturing of compliant elements with variable stiffness, which have been adopted to increase the locomotion efficiency in robots with different leg configurations, e.g. in a hopping robot using a segmented leg [13], or in a hexapod robot with C-shaped legs [14]. However, the gait optimization in those works has been mostly based on empirical work on the robots.

This paper provides a numerical analysis of the influence of variable leg elasticity on the stability of quadrupedal gaits. A simplified quadrupedal model with compliant legs and

This project has received funding from the European Research Council (ERC) under the European Union's Horizon 2020 research and innovation programme with the grant agreement No 835284, M-Runner.

[1]F. Del Fatti is with Politecnico di Milano, Milan, Italy federico.delfatti@mail.polimi.it

[2]A. Sesselmann and M. Roa are with the Institute of Robotics and Mechatronics, German Aerospace Center (DLR), 82234 Wessling, Germany anna.sesselmann@dlr.de, maximo.roa@dlr.de

 DOI: 10.1109/IROS47612.2022.9982204

fixed stiffness, initially introduced in [15], is used to obtain a wide range of emerging gaits. An optimization procedure is then employed in order to characterize the optimum parameters for maximizing the stability of the gaits for a similar model, but now endowed with variable elasticity. The stability for the models with fixed and variable stiffness is compared, verifying that the variable stiffness can effectively improve the stability for quadrupedal gaits.

II. Quadruped Passive Dynamical Model

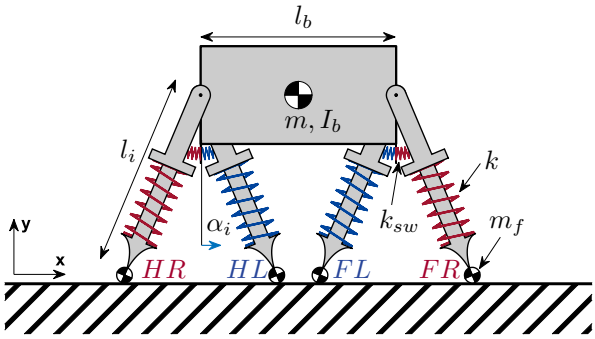

Fig. 2: Quadrupedal model with compliant legs and hips.

To analyze the variable leg stiffness, we start with the model with compliant legs and hips introduced in [15]. This planar model, shown in Fig. 2, has a rigid trunk of mass m, length l_b, and rotational inertia I_b. The legs are massless, with resting length l_0, stiffness k, and foot mass m_f. Each leg i is connected to the corresponding hip by a torsional spring of stiffness k_{sw}. This spring is unloaded with leg angle $\alpha_i = 0$ when the leg is perpendicular to the trunk. Here, $i \in [FR, FL, HR, HL]$, with FR being the front right leg, FL the front left leg, HR the hind right leg, and HL the hind left leg. The robot state is described by $q = [x, y, \psi, \alpha_{FR}, \alpha_{FL}, \alpha_{HR}, \alpha_{HL}]$ and their corresponding derivatives $\dot{q}$, where x and y are the horizontal and vertical coordinates of the trunk center of mass (CoM), and ψ is the trunk rotation angle. The hip coordinates are given by $x_{i,hip}$ and $y_{i,hip}$. The passive model becomes conservative by imposing $m_f \to 0$ and $k_{sw} \to 0$, thus avoiding energy losses from leg impact with the ground. Following [9], to consider the passive swing for legs not in contact with the ground, a leg swing frequency is introduced as

$$\omega = \sqrt{\frac{k_{sw}}{m_f\, l_0^2}}\ , \tag{1}$$

where ω is a finite constant parameter. Each leg is sequentially changing between two discrete phases:

- In *stance phase* the leg is in contact with the ground, can be compressed, and exerts force on the trunk and on the ground. An ideal foot-ground contact is introduced. Therefore, the horizontal and vertical position of the foot are constant during this phase.
- In *swing phase* the leg is not in contact with the ground, is uncompressed, and moves due to the passive dynamics ruled by the trunk motion and by the swing frequency ω. Swinging legs do not influence the motion of the trunk, as the leg is massless and the foot mass is infinitesimal.

The switch from one discrete phase into the other is triggered by *event functions*, which monitor two events:

- At *touchdown* the leg contacts the ground. The swing phase ends and the stance phase begins when $e_{td} = l_0 \cos(\alpha_i) - y$ crosses zero.
- At *liftoff* the leg loses contact with the ground and switches from stance to swing phase when the event function $e_{lo} = \sqrt{(x_{i,hip} - s_i)^2 + y_{i,hip}^2} - l_0$ crosses zero, i.e. when the leg is completely unloaded. Here, s_i is the horizontal coordinate of the foot at touchdown..

The hybrid dynamics of the model is characterized by *motion phases* with different contact patterns. When an event is detected for any leg, the leg contact state changes, a transition between two motion phases happens, and the system dynamical equations are modified to account for the influence of the new contact. All system variables are continuous between two consecutive motion phases, with the possible exception of the leg angular velocity at touchdown, which can be discontinuous if the velocity in the swing phase is not equivalent to the one imposed by the stance phase.

The dynamical equations of the model depend on the force/torque acting at the CoM. If the i^{th} leg is in swing phase, it exerts no forces on the trunk. In stance phase, however, the horizontal and vertical force components $F_{x,i}$ and $F_{y,i}$, are given by

$$\begin{aligned} F_{x,i} &= -k(l_i - l_0)\sin(\alpha_i) \\ F_{y,i} &= k(l_i - l_0)\cos(\alpha_i) \end{aligned} \tag{2}$$

with l_i the leg length. The forces from the front and hind legs act on the trunk via the hip joints. The dynamic equations of the trunk are then

$$\begin{aligned} m\ddot{x} &= F_{x,FR} + F_{x,FL} + F_{x,HR} + F_{x,HL} \\ m\ddot{y} &= F_{y,FR} + F_{y,FL} + F_{y,HR} + F_{y,HL} \\ I_b\ddot{\psi} &= 0.5\, l_b\, (m\ddot{y}\cos(\psi) - m\ddot{x}\sin(\psi)) \end{aligned} \tag{3}$$

The swing leg dynamics is described by

$$\ddot{\alpha}_i = -\frac{\ddot{x}_{i,hip}\cos(\alpha_i)}{l_0} - \frac{g + \ddot{y}_{i,hip}\sin(\alpha_i)}{l_0} - \frac{k_{sw}\alpha_i}{m_f l_0}\ , \tag{4}$$

with g the gravitational acceleration. Finally, the angles of the legs in contact are

$$\alpha_i = \text{atan}\left(\frac{s_i - x_{i,hip}}{y_{i,hip}}\right)\ . \tag{5}$$

III. Methods to Analyze Emerging Gaits

The conservative model introduced in the previous section displays multiple inherent passive gaits. These gaits are periodic motions, which are defined by their footstep sequence (FSS). As an example, Fig. 3 shows the sequence of motions for the first half of a pace stride, and Fig. 4 displays the corresponding FSS. For each leg, the ground contact during one stride is visualized as a percentage of the

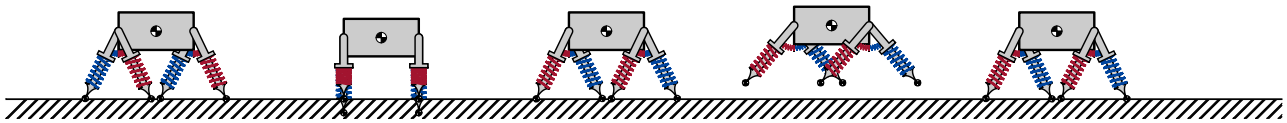

Fig. 3: Visualization of the pace forward gait.

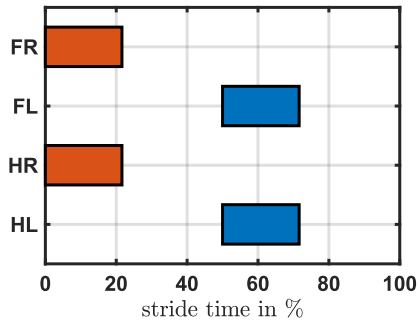

Fig. 4: Footstep sequence of the pace forward gait.

total stride time. This section introduces the method to find such emergent passive gaits and to assess their stability.

A. Finding Periodic Solutions

The search of passive periodic motions emerging from the described model is reformulated as a boundary value problem (BVP), as suggested by [16]. The state variables q_j and their derivatives $\dot{q}_j$ at the start of each motion phase j (see section II) and the phase duration T_j are collected in the expanded state vector $Z_j = [q_j, \dot{q}_j, T_j]$, thus the full motion is specified by $\mathbf{Z} = [Z_0, Z_1, ..., Z_m]$ where m is the number of phases of the stride. For each phase, adimensional time $\tau_j \in [0, 1]$ is introduced as

$$\tau_j = \frac{t_j - t_{j,start}}{t_{j,end} - t_{j,start}} = \frac{t_j - t_{j,start}}{T_j} \ , \tag{6}$$

where t_j is the time variable of the j^{th} phase and $t_{j,start}$, $t_{j,end}$ indicate the corresponding initial and final time. In dimensionless time, $\tau = 0$ and $\tau = 1$ correspond to the start and end of each phase, respectively. The state space formulation $\dot{\mathbf{Z}} = \mathbf{f}(\mathbf{Z}(\tau))$ contains the dynamical equation of each phase with $\dot{T}_j = 0$. Suitable boundary conditions $\mathbf{G}$ are introduced to impose (i) continuity of the motion (state space variables are equal at the transition between phases, i.e., $\mathbf{Z}_{j+1}(0) = \mathbf{Z}_j(1)$, except for the time duration of the phase), (ii) verification of the transition equations (Section II), and (iii) the periodicity of the overall motion (i.e., $\mathbf{Z}_1(0) = \mathbf{Z}_m(1)$). The complete BVP is given by

$$\begin{cases} \dot{\mathbf{Z}} = \mathbf{f}(\mathbf{Z}(\tau)) \\ \mathbf{G}(\mathbf{Z}(0), \mathbf{Z}(1)) = 0 \\ \tau \in [0, 1] \end{cases} . \tag{7}$$

A shooting method is utilized to solve the BVP. This method creates a guess for the initial value of the expanded state vector $\mathbf{Z}(0)$, integrates the state space formulation, and checks if the boundary conditions are satisfied. Solutions of the BVP correspond to periodic gaits emerging from the quadrupedal model.

B. Discovering Solution Branches

Periodic solutions of conservative systems are not isolated. This means that a neighbouring periodic solution, $\mathbf{Z}_{n+1}$, can be produced with an infinitesimal perturbation of the original solution $\mathbf{Z}_n$. We use a continuation algorithm to formulate a guess for a neighboring solution $\mathbf{Z}^g_{n+1}$ as

$$\mathbf{Z}^g_{n+1} = \mathbf{Z}_n + d\,\frac{\mathbf{Z}_n - \mathbf{Z}_{n-1}}{|\mathbf{Z}_n - \mathbf{Z}_{n-1}|} \ , \tag{8}$$

where d is the step length between the two periodic solutions. The BVP solution of this guess is $\mathbf{Z}_{n+1}$. Repetition of the continuation algorithm discovers the continuous neighborhood of periodic motions of the conservative system, which is called a solution branch. All solutions of a branch have the same FSS, but have different system energies. During the branch discovery, the step length d is adapted to the curvature of the branch, increasing or decreasing it for low or high curvature in the branches, respectively.

C. Searching for Bifurcations

The eigenvalues of the Jacobian matrix $\mathbf{J}$ of the constraints $\mathbf{G}$ are used to discover solutions that belong to multiple solution branches. The Jacobian matrix $\mathbf{J}$ can be calculated as

$$\mathbf{J} = \frac{d\mathbf{G}(\mathbf{Z}_0, \mathbf{Z}_1)}{d\mathbf{Z}(0)} \tag{9}$$

Applying the chain rule leads to

$$\mathbf{J}^k = \frac{\partial \mathbf{G}}{\partial \mathbf{Z}^k(0)} + \frac{\partial \mathbf{G}}{\partial \mathbf{Z}^k(1)} \cdot \frac{\partial \mathbf{Z}^k(1)}{\partial \mathbf{Z}^k(0)} \tag{10}$$

where k indicates the considered element on the $\mathbf{Z}$ state variable vector and the corresponding column of $\mathbf{J}$. The first factor $\frac{\partial \mathbf{G}}{\partial \mathbf{Z}^k(0)}$ and the second one $\frac{\partial \mathbf{G}}{\partial \mathbf{Z}^k(1)}$ can be computed knowing the formulation of $\mathbf{G}$. To calculate the third factor, we introduce the $\mathbf{\Lambda}$ matrix, defined as

$$\mathbf{\Lambda}_i(\tau) = \frac{\partial \mathbf{Z}_i(\tau)}{\partial(\mathbf{Z}_i(0))}. \tag{11}$$

Differentiating with respect to the dimensionless time gives

$$\dot{\mathbf{\Lambda}}_i(\tau) = \frac{\partial \dot{\mathbf{Z}}_i(\tau)}{\partial \mathbf{Z}_i(0)}. \tag{12}$$

Note from (7) that the term $\dot{\mathbf{Z}}_i(\tau)$ is equivalent to $\mathbf{f}_i(\mathbf{Z}_i(\tau))$. Introducing it in (12) and applying the chain rule leads to:

$$\dot{\mathbf{\Lambda}}_i(\tau) = \frac{\partial \mathbf{f}_i(\mathbf{Z}_i(\tau))}{\partial \mathbf{Z}_i(\tau)} \cdot \frac{\partial \mathbf{Z}_i(\tau)}{\partial \mathbf{Z}_i(0)} = \frac{\partial \mathbf{f}_i(\mathbf{Z}_i(\tau))}{\partial \mathbf{Z}_i(\tau)} \cdot \mathbf{\Lambda}_i(\tau). \tag{13}$$

Given an initial condition, the matricial equation (13) can be integrated with respect to τ. Due to the definition of the Λ matrix (11), its value for $\tau = 0$ is the identity matrix $\boldsymbol{I}$. To calculate $\Lambda_i(1)$ we must solve the initial value problem

$$\begin{cases} \mathbf{\Lambda}_i(1) = \int_0^1 \frac{\partial \mathbf{f}_i(\mathbf{Z}_i(\tau))}{\partial \mathbf{Z}_i(\tau)} \cdot \mathbf{\Lambda}_i(\tau)\, d\tau \\ \mathbf{\Lambda}_i(0) = \boldsymbol{I} \end{cases} \tag{14}$$

The resulting $\mathbf{\Lambda}_i(1)$ term is the searched third factor of (10).

For each periodic solution at least one zero eigenvalue of $\mathbf{J}$ exists. The associated eigenvector is tangential to the solution branch. If more than one zero eigenvalue is present, the solution is called a bifurcation point. Each eigenvector that is associated with a zero eigenvalue is tangential to a separate solution branch. A monitoring algorithm runs in parallel to the branch discovery, analyzing the eigenvalues of $\mathbf{J}$ to detect bifurcation points. A bifurcation point is the origin for a new gait, which displays a new FSS due to a break in the gait symmetry.

D. Assessing Stability

The stability of the solutions is computed utilizing the Poincare section, the Poincare Map, and the Monodromy matrix [17]. The *Poincare section* $\mathbf{X} \in \mathbb{R}^n$ is the state space intersection of a periodic orbit with a lower-dimensional subspace. In the Poincare section, the gait can be characterized with a reduced set of parameters, i.e. the n independent parameters describing this instant of the motion. The *Poincare map* $\mathbf{P}(\mathbf{X})$ is a function that maps the initial condition $\mathbf{X}$ of the system at the Poincare section to the system state after one stride. For a periodic orbit, $\mathbf{P}(\mathbf{X}) = \mathbf{X}$. The *Monodromy matrix* $\mathbf{M}$ is the Jacobian matrix of the Poincare map with respect to the corresponding Poincare section,

$$\mathbf{M} = \frac{\partial \mathbf{P}(\mathbf{X})}{\partial \mathbf{X}} \tag{15}$$

The eigenvalues of the Monodromy matrix are called *Floquet multipliers*, λ. If all Floquet multipliers have absolute values lower than one, any perturbation of the Poincare section is attenuated stride after stride and the system is asymptotically stable. However, if at least one eigenvalue has an absolute value greater than one, a perturbation drives the system away from the periodic orbit, i.e. the system is unstable.

IV. Emerging Gaits: Motion and Stability

Using the quadrupedal model described in section II and the methods introduced in section III, it is possible to characterize several gaits observed in nature. In order to obtain general results, all variables and model parameters are adimensionalized with respect to the resting leg length l_0, the gravitational acceleration g, and the body mass m. For our model, we chose as parameters an adimensional leg stiffness $K = 10$, leg swing frequency $\Omega = \sqrt{5}$, and body rotational inertia $I_b = 1.2$, following the values used in [18]. Table I gives an overview of gaits discovered for this model, and the attached video shows examples of these gaits.

TABLE I: Overview of passive gaits discovered with the quadrupedal passive dynamical model.

Acronym	Description	Bifurcate from	Symmetrical/ Asymmetrical
PP	Pace in place	-	sym
$P1$	Pace forward with positive $\dot{\alpha}_{TD}$	PP	sym
$W1_{P1}$	Walking gait	$P1$	sym
$W2_{P1}$	Single-foot run	$P1$	sym
$P2$	Pace forward with negative $\dot{\alpha}_{TD}$	PP	sym
$W1_{P2}$	Walking gait	$P2$	sym
$W2_{P2}$	Single-foot run	$P2$	sym
$H2_W$	Walking pace-like gait with double humped force profile	-	sym
TP	Trot in place	-	sym
$T1$	Trot forward with positive $\dot{\alpha}_{TD}$	TP	sym
$W1_{T1}$	Walking gait	$T1$	sym
$W2_{T1}$	Single-foot run	$T1$	sym
$T2$	Trot forward with negative $\dot{\alpha}_{TD}$	TP	sym
$W1_{T2}$	Walking gait	$T2$	sym
$W2_{T2}$	Single-foot run	$T2$	sym
$H2_{TW}$	Walking trot-like gait with double humped force profile	-	sym
PRP	Pronk in place	-	asym
PR	Pronk forward	PRP	asym
B	Bound	PR	asym
HB	Half bound	B	asym
G	Gallop	HB	asym

A. Symmetrical Gaits

A symmetrical gait has the footfalls of the right and left leg of each pair (front or hind) separated by 50% of the stride time. Animals usually adopt these gaits for low to medium velocity locomotion. The simplest of these gaits is the pace in place (PP) gait. From this gait, different behaviors emerge, as visualized in Fig. 5, including the pace gaits $P1$ and $P2$, and also walking gaits $W1$ and single-foot running gaits $W2$.

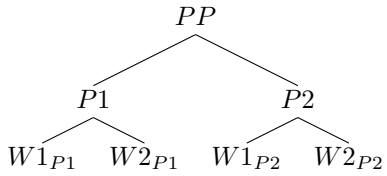

Fig. 5: Symmetrical gaits emerging from the pace in place gait PP.

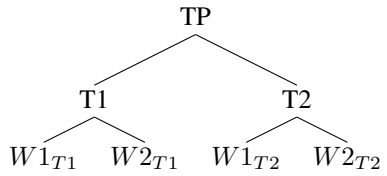

Fig. 6: Symmetrical gaits emerging from the trot in place gait TP.

From the trot in place branch, TP, the model exhibits trot gaits $T1$ and $T2$. A walking gait with a double-humped force profile, $H2$, can also be obtained for the model. The relation of the gaits that emerge from the trot in place TP gait are visualized in Fig. 6.

To compare with gaits obtained in nature, we make use of the Hildebrand plot. This plot characterizes the gaits by the footstep sequence; similar gaits will belong to the same region of the graph, thus leading to a visual characterization of the locomotion gaits. Fig. 7 overlays the symmetrical gaits that emerge from the quadrupedal model on a *Hildebrand symmetrical gaits plot* [1]. The found branches of solution intersect the regions of the natural gait cloud corresponding to the most common gaits observed in nature [19]. The branches extend also to regions corresponding to very short leg-ground contact time. These are high speed gaits that have no correlation in nature due to their high instability. Animals at high speed instead tend to adopt asymmetrical gaits.

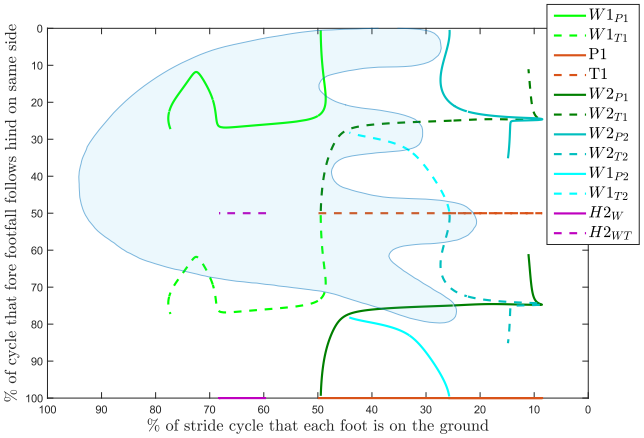

Fig. 7: Overlay of the emerging symmetrical gaits on the Hildebrand symmetrical gait plot. The cyan region of the plot represents the natural gaits observed in mammals.

B. Asymmetrical Gaits

In asymmetrical gaits, the left and right leg of each pair have different roles. The first leg of a pair to touch down is called *leading leg*, and the other one is the *trailing leg*. In a transverse gallop, for instance, the leading legs of each pair are on the same side. In contrast, in a rotary gallop the leading legs are on different sides. In bounding gaits, both legs of each pair move in unison.

With the presented model, different asymmetrical gaits emerge, including pronk, half bound, bound and gallop. Fig. 8 visualizes those main natural gaits in a *Hildebrand asymmetrical gaits plot* [1]. Note that most of the characterized gaits are outside the corresponding regions of the natural gaits. That difference is related to the very short support time with respect to the aerial time for the gaits emerging from the quadrupedal model. This causes the emerging gaits to appear in the right part of the Hildebrand asymmetrical plot, while natural gaits are mainly concentrated on the left part, as they display longer suspension times.

C. Gait Stability

All the emerging passive gaits of the quadrupedal model are unstable, as for all of them the absolute value of the maximum Floquet multiplier, λ_{max}, is larger that one (Fig. 9). In

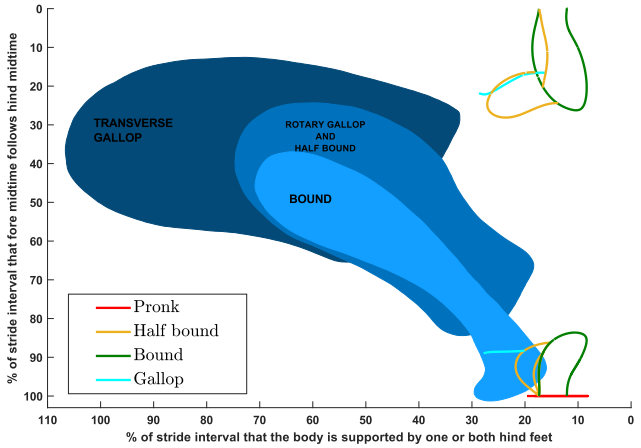

Fig. 8: Overlay of the emerging asymmetrical gaits on the Hildebrand asymmetrical gait plot. The blue regions represent natural gaits of mammals.

general, a lower synchronization of the legs improves gait stability. This means that in general overall gait stability seems to improve when the number of bifurcations between the gait and the corresponding in-place gait is higher. For instance, single-foot gaits are more stable than pace or trot gaits. Similarly, for asymmetrical gaits the general stability improves progressively with each bifurcation from the pronk, to bound, to half-bound, and to gallop gaits. However, stability highly varies at different horizontal velocities for the different gaits, as can be noticed by the large variation of λ_{max} in Fig. 9.

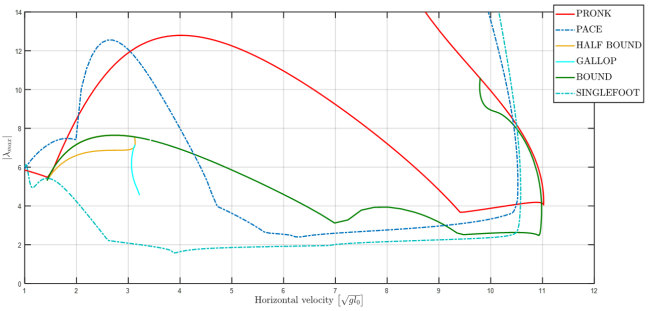

Fig. 9: Comparison of the maximum Floquet multipliers, λ_{max}, for the emerging gaits.

D. Optimized Stability Through Variable Elastic Parameters

The analysis above showed that the quadrupedal model with fixed parameters leads to unstable gaits (Fig. 9). In principle, optimizing the choice of the fixed parameters leads to an improvement in locomotion stability for a specific gait at a specific horizontal velocity, e.g. as performed for trotting using a segmented leg model in [20]. To obtain a more generic solution, a variable elasticity is now introduced in the model, by allowing the leg stiffness K to have a range of variation. We also endow the model with variable swing frequency Ω, which would correspond to a variable

hip stiffness. The goal is to determine if by adopting such variable elasticity it is possible to improve the locomotion stability for a wide range of horizontal velocities and for different gaits.

Discovered gaits might display large differences in stability along the solution branch, as only one solution can be found for each gait at a specific energy level for a model with fixed parameters. In other words, the neighborhood of solutions for one gait is one-dimensional (it lies on one branch). However, in the case of variable parameters, an infinite number of solutions of a specific gait can be found at a given energy level. This means that an optimal parameter set for maximizing gait stability can be found for every gait and for every energy level.

System stability is directly correlated to the maximum absolute value of the Floquet multipliers, λ_{max}, and therefore this value is used as objective function. For a given solution branch of the original model, an optimization procedure is performed using this objective function to find an optimal set of parameters that maximizes stability. The elastic parameters (K and Ω) for a fixed point on the original branch at a given energy level are perturbed, the limit cycle is computed for this set of parameters, and the process is repeated until a local minima in λ_{max} is obtained, i.e, until obtaining a set of parameters that maximize the system stability. The process is applied to all the original branch. Note that the method does not guarantee that the local minimum corresponds to the global minimum at a given energy level.

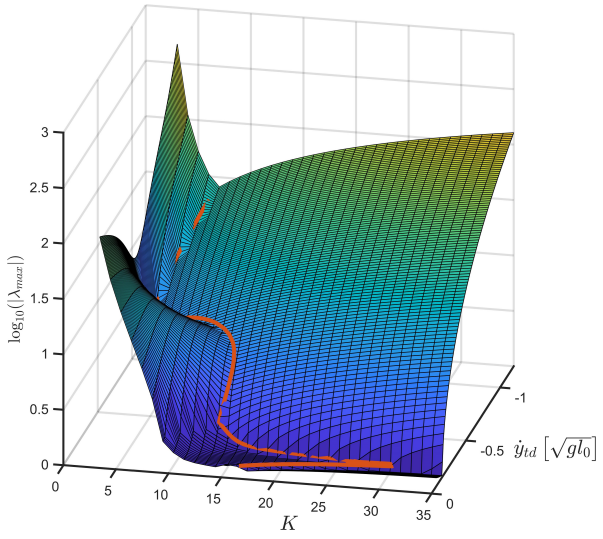

Fig. 10: Visualization of the optimization procedure of the pace in place branch for the model with variable stiffness.

Figure 10 shows a visualization of the optimization procedure for the model with variable leg stiffness during the pace in place gait. In this case, the optimization method is employed to search for the optimal stiffness for different values of the vertical velocity at touchdown. The surface shows the behavior of λ_{max} using different leg stiffness and different vertical velocities at touchdown. The solid red curve represents the resulting optimal value of stiffness and the corresponding λ_{max} value for each vertical velocity. This optimization method has been applied to the pace and bound gaits, as shown in the next subsections. The pace gait shows the highest stability of all symmetrical gaits, and extends over a wide range of horizontal velocities. The bound gait shows the highest correlation of all asymmetrical gaits of this model with the natural gaits, and is the only emerging branch of the asymmetrical gaits crossing the corresponding region of natural gaits in Fig. 8.

E. Improved Pace Stability

The optimization procedure was initially applied to the pace branch. The optimization results are reported in Fig. 11, showing that the optimal leg stiffness linearly increases with the forward velocity, which directly corresponds to system energy. Note how the variable stiffness greatly improves the stability of the gait in comparison to the stability of the pace gait in the model with constant stiffness (black line in Fig. 11).

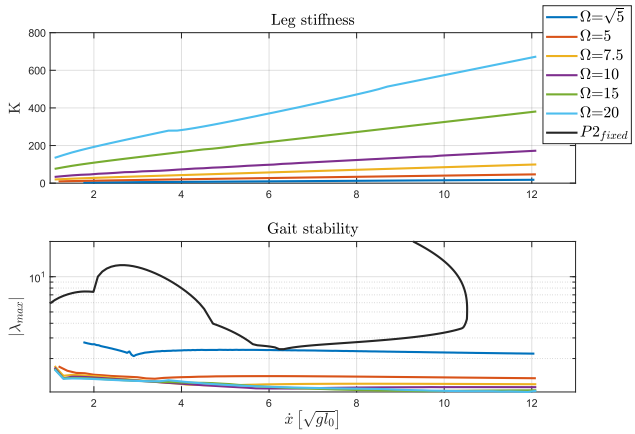

Fig. 11: Stability optimization of the pace gait $P2$ with variable leg stiffness K for different fixed swing frequencies Ω.

These results hold for the analyzed swing frequencies. Additionally, the results show that higher swing frequencies are associated with better system stability, as well as a reduction in the vertical oscillations of the trunk, as observed in Fig. 12a. Furthermore, it also slightly reduces the maximum forces per leg (Fig. 12b). In fact, when considering a model with variable leg swing frequency Ω, very high values of Ω are necessary to improve the gait stability. However, in reality, the presence of a finite foot mass and leg inertia limit the maximum attainable value of Ω. Our results indicate that if a maximum value of Ω is introduced and an optimization with variable leg stiffness and leg swing frequency is performed, the optimal stability is achieved using the maximum Ω, and a leg stiffness that increases with the horizontal velocity (Fig. 11). Therefore, the optimal results are achieved for a model with variable stiffness K and constant leg swing frequency Ω, which is set to the maximum possible value. Finally, Fig. 13 visualizes the optimized pace gait $P2$ for different swing frequencies. Note that the maximum leg angle is smaller for higher swing frequencies.

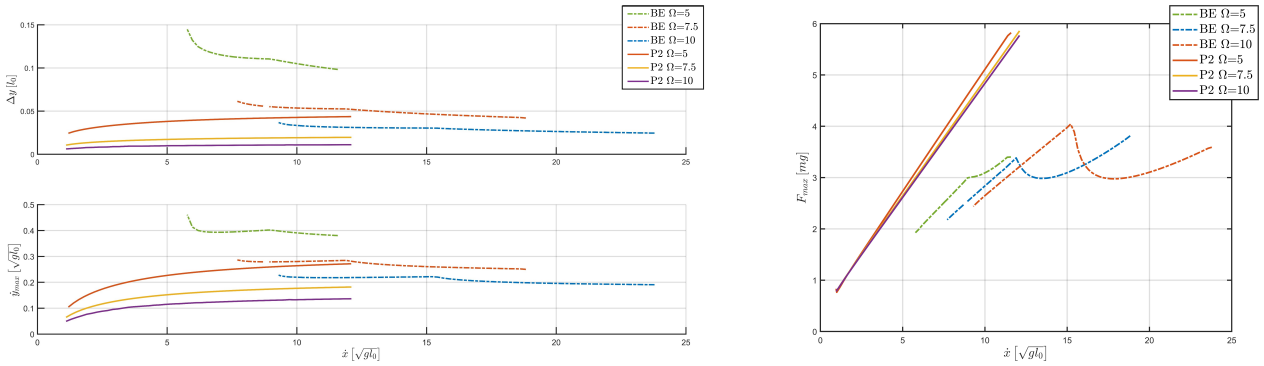

(a) Vertical displacement and maximum velocity

(b) Maximum forces per leg

Fig. 12: Comparison of the optimized BE and $P2$ gaits with variable stiffness at different leg swing frequencies.

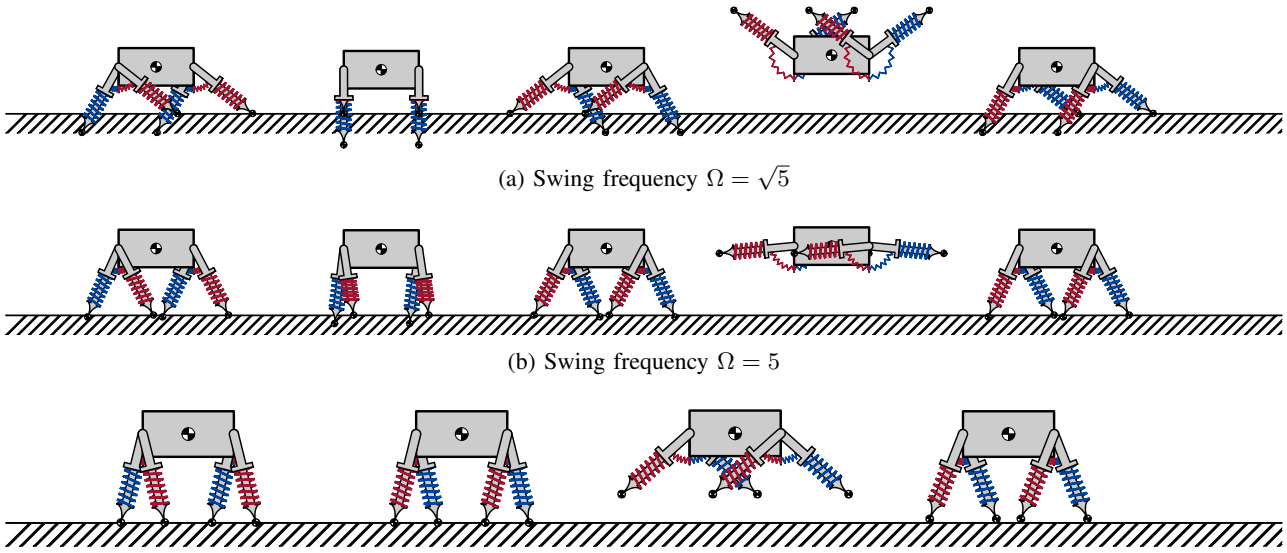

(a) Swing frequency $\Omega = \sqrt{5}$

(b) Swing frequency $\Omega = 5$

(c) Swing frequency $\Omega = 10$

Fig. 13: Optimized pace forward gait $P2$ with variable leg stiffness K for different constant swing frequencies Ω at the same horizontal velocity of $\dot{x} = 10\sqrt{gl_0}$. The attached video illustrates these gaits.

F. Improved Bound Stability

For the stability optimization of the bound gait, the results follow the same observations obtained for the pace gait optimization. Highest stability is achieved when the leg stiffness K is linearly increasing with horizontal velocity. However, at a certain forward velocity the optimal leg stiffness starts decreasing with increasing horizontal velocities. On the other hand, for higher swing frequencies, the overall gait stability is higher. A higher leg swing frequency reduces both the rotation and the vertical oscillations of the trunk (Fig. 14 and Fig. 12a).

Furthermore, a higher leg swing frequency is associated with less leg compression in stance and a corresponding higher body position during the stride, as observed in Fig. 13. Finally, a higher leg swing frequency reduces the maximum force for leg, as shown in Fig. 12b. Note also that the optimized bound gait has a lower maximum force per leg in comparison to the pace gait, as a result of the synchronous motion of the front and hind pair legs.

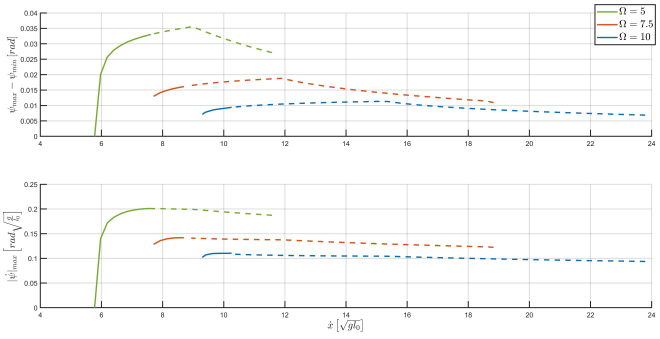

Fig. 14: Rotational displacement and maximum velocity for the bound gait.

A comparison of the stability of the optimized pace and bound gaits is given in Fig. 15. Note that the optimized bound gaits show higher stability than the pace gaits, but both gaits exist only for a certain range of horizontal velocities, low/medium for the pace, and medium/high for bound gaits.

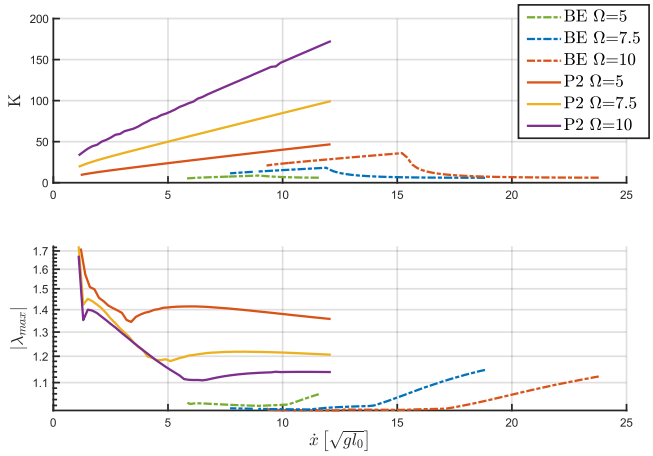

Fig. 15: Comparison of the optimized pace (P2) and bound (BE) gaits with variable leg stiffness K for different constant swing frequencies Ω.

V. Final Discussion

This paper has analyzed the stability of emerging gaits for a fully passive quadrupedal model with compliant legs and hips. The quadrupedal model with fixed parameters was introduced in [18], where the emerging gaits were initially studied. The model in fact exhibits the most common quadrupedal mammalian gaits observed in nature [1]. This paper extended such results with a stability analysis of the emerging gaits. We observed that the break of symmetry associated with the bifurcation of new solution branches improves gait stability. However, high variations in the stability at different horizontal velocities have been observed.

We had previously demonstrated that tuning the system parameters improves the gait stability for a specific gait (trotting) at specific velocities [20]. However, using a model with fixed parameters it is not possible to optimize the stability for a wide range of velocities. In this work we extended the model from [18] with variable leg stiffness and leg swing frequency (corresponding to variable hip stiffness), and used an optimization algorithm to find the optimal leg stiffness and swing frequency for a desired velocity and gait, thus leading to an enhanced locomotion stability. Our results show that the adoption of the highest possible leg swing frequency and of a leg stiffness that increases with the horizontal velocity significantly improves the gait stability.

The presented approach allows an optimization of the variable stiffness parameters, which can then be adopted for the online control of a real robot during locomotion. The dynamical model utilized here is however highly simplified, and the obtained results are indicative of a general dynamic behavior, but the translation of results to the real robot could be difficult. The adoption of a more detailed model with segmented legs configuration, more similar to the legs commonly used in quadrupedal robots (e.g. as in [20]), could facilitate such translation of results. The accuracy of the model used here could be increased by introducing a finite foot mass as well as dampers in parallel to the leg springs, in order to model the energy losses associated with the foot impact and the friction. A simple bang-bang actuation, acting on the leg rest length, could be adopted to reintroduce the energy lost during the cycle. Further work could improve the analysis by considering stability in three dimensions, non-flat ground, and varying forward velocity, and investigating if the continuation and bifurcation analysis could characterize the gaits of non-conservative models.

References

[1] M. Hildebrand, "The quadrupedal gaits of vertebrates," *BioScience*, vol. 39, no. 11, pp. 766–775, 1989.

[2] E. M. Summerside, R. Kram, and A. A. Ahmed, "Contributions of metabolic and temporal costs to human gait selection," *J. of The Royal Society Interface*, vol. 15, no. 143, p. 20180197, 2018.

[3] V. Caggiano, R. Leiras, H. Goñi-Erro, D. Masini, C. Bellardita, J. Bouvier, V. Caldeira, G. Fisone, and O. Kiehn, "Midbrain circuits that set locomotor speed and gait selection," *Nature*, vol. 553, no. 7689, pp. 455–460, 2018.

[4] G. A. Cavagna, N. C. Heglund, and C. R. Taylor, "Mechanical work in terrestrial locomotion: two basic mechanisms for minimizing energy expenditure," *American J. of Physiology-Regulatory, Integrative and Comparative Physiology*, vol. 233, no. 5, pp. R243–R261, 1977.

[5] M. Hutter, C. Gehring, D. Jud, A. Lauber, C. Dario, V. Tsounis, J. Hwangbo, K. Bodie, P. Fankhauser, M. Bloesch, R. Diethelm, S. Bachmann, A. Melzer, and M. Hoepflinger, "ANYmal - a highly mobile and dynamic quadrupedal robot," *IEEE/RSJ Int. Conf. on Intelligent Robots and Systems*, pp. 38–44, 2016.

[6] M. Hutter, C. Gehring, M. Bloesch, M. A. Hoepflinger, C. D. Remy, and R. Siegwart, "Starleth: A compliant quadrupedal robot for fast, efficient, and versatile locomotion," *Adaptive Mobile Robotics*, p. 483–490, 2012.

[7] R. Blickhan, "The spring-mass model for running and hopping," *J. of biomechanics*, vol. 22, no. 11-12, pp. 1217–1227, 1989.

[8] H. Geyer, A. Seyfarth, and R. Blickhan, "Compliant leg behaviour explains basic dynamics of walking and running," *Proc. Royal Society B: Biological Sciences*, vol. 273, no. 1603, pp. 2861–2867, 2006.

[9] Z. Gan, Y. Yesilevskiy, P. Zaytsev, and C. D. Remy, "All common bipedal gaits emerge from a single passive model," *J. of The Royal Society Interface*, vol. 15, no. 146, p. 20180455, 2018.

[10] Z. Gan, T. Wiestner, M. Weishaupt, N. Waldern, and D. Remy, "Passive dynamics explain quadrupedal walking, trotting, and tölting," *J. of computational and nonlinear dynamics*, vol. 11, no. 2, 2016.

[11] A. Albu-Schäffer and C. Della Santina, "A review on nonlinear modes in conservative mechanical systems," *Annual Reviews in Control*, vol. 50, pp. 49–71, 2020.

[12] C. Richard Taylor, "Why change gaits? recruitment of muscles and muscle fibers as a function of speed and gait," *American Zoologist*, vol. 18, no. 1, pp. 153–161, 1978.

[13] H. Q. Vu, H. Hauser, D. Leach, and R. Pfeifer, "A variable stiffness mechanism for improving energy efficiency of a planar single-legged hopping robot," in *Int. Conf. on Advanced Robotics*, 2013, pp. 1–7.

[14] K. C. Galloway, J. E. Clark, M. Yim, and D. E. Koditschek, "Experimental investigations into the role of passive variable compliant legs for dynamic robotic locomotion," in *IEEE Int. Conf. on Robotics and Automation*, 2011, pp. 1243–1249.

[15] Z. Gan and C. D. Remy, "A passive dynamic quadruped that moves in a large variety of gaits," *IEEE/RSJ Int. Conf. Intelligent Robots and Systems*, pp. 4876–4881, 2014.

[16] A. Merker, D. Kaiser, and M. Hermann, "Numerical bifurcation analysis of the bipedal spring-mass model," *Physica D: Nonlinear Phenomena*, vol. 291, pp. 21–30, 2015.

[17] G. Teschl, *Ordinary Differential Equations and Dynamical Systems*, 2012.

[18] Z. Gan, "Exploring passive dynamics in legged locomotion," Ph.D. dissertation, University of Michigan, 2018.

[19] M. Hildebrand, "The quadrupedal gaits of vertebrates," *BioScience*, vol. 39, no. 11, p. 766–775, 1989.

[20] L. Boffa, A. Sesselmann, and M. A. Roa, "Quadrupedal template model for parametric stability analysis of trotting gaits," in *IEEE/RSJ Int. Conf. on Intelligent Robots and Systems*, 2021, pp. 916–922.